Totten Glacier subglacial hydrology determined from geophysics and modeling

C. F. Dow[a,], F. S. McCormack[b], D. Young[c], J. Greenbaum[c], J. Roberts[d,e], D. Blankenship[c]

[a]*Department of Geography and Environmental Management, University of Waterloo, Waterloo, ON, Canada*
[b]*Institute for Marine and Antarctic Studies, University of Tasmania, Hobart, Tasmania, Australia*
[c]*Institute for Geophysics, Jackson School of Geosciences, University of Texas at Austin, Austin, TX, USA*
[d]*Australian Antarctic Division, Kingston, Tasmania, Australia*
[e]*Antarctic Climate & Ecosystems Cooperative Research Centre, University of Tasmania, Hobart, Tasmania, Australia*

Abstract

Aurora Subglacial Basin (ASB), which feeds Totten Glacier, is a marine basin lying below sea level and contains up to 3.5 m of global sea level equivalent. Rates of future sea level rise from this area are primarily dependent on the stability of Totten Ice Shelf and the controls on ice flow dynamics upstream of the grounding line, both of which may be influenced by subglacial hydrology. We apply the GlaDS subglacial hydrology model to ASB to examine whether the spatial patterns of distributed and efficient drainage systems impact the dynamics of Totten Glacier. We determine the most appropriate model configuration from our series of sensitivity tests by comparing the modeled basal water pressure and water depth results with specularity content data. Those data are derived from ICECAP radar surveys over the same

Email address: christine.dow@uwaterloo.ca (D. Blankenship)

region and represent regions of basal water accumulation. The best match between simulated basal hydrology properties and specularity content shows a strong correspondence in regions of distributed water in the ASB troughs for both water depth and water pressure, but weak correspondence between water depth and specularity content near the grounding line. This may be due to the presence of several large channels draining over the grounding line into the head of Totten Ice Shelf, which are likely not as well represented in the specularity content data as distributed systems. These channels may have a significant impact on melt, and therefore the stability, of Totten Ice Shelf. Within ASB, regions of high water pressure and greater water accumulation correspond well with regions of faster ice flow, suggesting some control of basal hydrology on ice dynamics in this region.
Keywords: glacier hydrology, ice dynamics, East Antarctica, Totten Glacier,

1. Introduction

Totten Glacier is one of the regions of the East Antarctic Ice Sheet most vulnerable to a warming climate. The Totten catchment has been observed to be losing mass at approximately $7\,\mathrm{Gt\,a^{-1}}$ over recent decades, of which 73% is attributed to ice sheet dynamics (Li et al., 2016). Totten Glacier has the highest mass flux over the grounding line in the East Antarctic, with Totten Ice Shelf thinning by $1.9\,\mathrm{m\,a^{-1}}$ over the period 2003-2009 (Pritchard et al., 2009) but also showing strong interannual variability (Paolo et al., 2015). The ice shelf has high basal melt rates of $\sim 10\,\mathrm{m\,a^{-1}}$ (Rignot et al., 2013; Gwyther et al., 2014) and is susceptible to infiltration of warm modified

circumpolar deep water that would cause even higher rates of basal melt, potentially leading to destabilization of the shelf (Greenbaum et al., 2015; Roberts et al., 2018a). If the buttressing effect of Totten Ice Shelf is removed (Fürst et al., 2016; Ritz et al., 2015), the ice in Aurora Subglacial Basin (ASB) that feeds this glacier will likely retreat into regions of reverse slopes below sea-level (Greenbaum et al., 2015; Aitken et al., 2016). Given that Totten Glacier holds back 3.5 m of sea level potential, retreat of this ice body could have significant global consequences (Greenbaum et al., 2015).

The subglacial hydrological system in the ASB has the potential to impact the stability of both Totten Glacier and Totten Ice Shelf. Mass loss from Totten Ice Shelf is highly spatially variable (Gwyther et al., 2014), with some regions of melt significantly impacting ice flow of Totten Glacier, especially near rumples just downstream of the grounding zone (Roberts et al., 2018a). It is unclear whether the driver of localized high melt is ocean-sourced, subglacially-sourced from water draining over the grounding line into the shelf cavity, or a combination of the two.

The basal hydrological system, which drives rates and locations of these drainage points could also facilitate fast ice flow through lubrication from high pressure water. The ASB has previously been characterized as having widespread distributed hydrological networks with almost 200 'lake-like' or water accumulation features (Wright et al., 2012). The majority of these features were identified as bright reflectors at the ice/bed interface in aerial geophysical radar that was flown over the region. Analysis of Ice, Clouds, and Land Elevation Satellite (ICESat) data over ASB has also demonstrated the presence of at least 2 active lakes that fill and drain over a period of 3-4.5

years (Smith et al., 2009). Hydraulic potential analysis of one of these lakes has determined that the water routing out of the lake can drain alternately into either Totten or Vanderford ice shelves with only a slight change in surface slope (Young et al., 2016), suggesting that the drainage system may be highly variable particularly at times of ice advance and retreat or changes in basal water pressure. Finally, ASB consists primarily of sedimentary rocks (Aitken et al., 2016), which may have implications for groundwater influx into the region and therefore hydrological development over longer (millennial) timescales (Siegert et al., 2018) due to aquifer loading and unloading over glacial cycles.

These studies of ASB suggest that the subglacial hydrological system is spatially and temporally variable and has the potential to be a dominant control on ice dynamics, and therefore the stability, of Totten Glacier. However, significant gaps remain in understanding the evolution of the ASB subglacial hydrological network, in particular the impact of spatially variable water pressures on the flow routing at the ice/bed interface along with the implications of efficient flow path development. We apply the Glacier Drainage System (GlaDS) model, a 2D subglacial hydrology model with distributed and channelized components, to the ASB region. We validate the model by comparing the estimates of water depth and hydraulic pressure with specularity content products derived from aerial geophysical radar data. Model results reveal characteristics of the hydrological system that appear to contribute directly to the dynamics and stability of Totten Glacier.

The aims of this study are threefold, with the first to use geophysical data to establish the most appropriate model parameters for this region;

having established the best model configuration, identify the location of high pressure areas that can be used as a proxy for regions likely to experience fast ice flow; and finally to determine the flux rates and locations of water inputs into Totten Ice Shelf cavity. We combine these three primary aims to address the role of subglacial hydrology in the stability of ASB and Totten Glacier.

2. Aurora Subglacial Basin

Aurora Subglacial Basin is located in the East Antarctic and feeds the highly dynamic Totten Glacier and the Vanderford Glacier (Fig. 1). For our analyses we also include the smaller Sabrina Subglacial Basin, which feeds into the eastern side of Totten Ice Shelf (Aitken et al., 2016). Surface ice velocity in the ASB region ranges from $<1\,\mathrm{m\,a^{-1}}$ up to $750\,\mathrm{m\,a^{-1}}$ at the grounding line of Totten Glacier. The size of the ice catchment is 570,000 km^2 and constitutes 6.5% of the East Antarctic Ice Sheet volume, with the potential to raise sea level by at least 3.5 m (Greenbaum et al., 2015). Furthermore, $\sim$ 51% of the basin is below sea level, with the southern end of Totten Glacier on a retrograde bed slope (Fretwell et al., 2013). Unlike other regions of the East Antarctic, the Totten Ice Shelf is subject to the impacts of warm modified Circumpolar Deep Water (Silvano et al., 2017), similar to ares of the West Antarctic that are already retreating potentially due to marine ice sheet instability (Joughin et al., 2014). These factors indicate that ASB is a primary candidate for future instability in the East Antarctic.

The International Collaborative Exploration of the Cryosphere by Airborne Profiling (ICECAP) project has run surveys between 2009 and 2018

collecting radar, surface laser altimetry and gravimetry data over ASB, accumulating an increasingly dense grid of data that can be processed into surface and basal digital elevation models (DEMs) along with maps of basal reflectivity (Wright et al., 2012) and specularity content (Schroeder et al., 2015). The radar data were collected with the High Capability Airborne Radar Sounder (HiCARS) which, along with processing techniques and associated measurement uncertainties, is described in Peters et al. (2007). To date, 104,640 km of flight lines have been completed over ASB by ICECAP (Blankenship et al., 2011, 2012, 2018; Roberts et al., 2018b).

3. Modeling approach

We use GLaDS to analyze the basal hydrological system of ASB. This model is described fully in Werder et al. (2013) and has been previously applied to Alpine glaciers (Werder et al., 2013), Greenland (Dow et al., 2018a; Gagliardini and Werder, 2018; Downs et al., 2018) and to ice streams and subglacial lake drainage analysis in the Antarctic (Dow et al., 2016, 2018b). This model reproduces development of a basal hydrological distributed sheet and channels on a finite element mesh. Exchange of water between the sheet that flows across the elements and channels that form along the element edges makes this a dynamic 2D model that is ideally applicable to Antarctic drainage systems. A key advantage of this model is the ability of channels to form and collapse due entirely to development of the drainage system rather than being prescribed during model initiation.

The ASB domain was constructed by assuming an overburden hydraulic potential and calculating the resulting catchment size. We refine the mesh

around the grounding line of Totten and Vanderford Glaciers and also in regions where negative effective pressures were obtained in initial testing. The grounding line of Totten Glacier is from Greenbaum et al. (2015) and smoothed due to limits for mesh refinement with this large catchment. The Vanderford Glacier grounding line is from Bindschadler et al. (2011). The mesh has 21,000 nodes and an outlet dirichlet water pressure boundary condition of overburden at the grounding lines. A zero flux condition is set for the remainder of the boundary. The minimum edge length is 0.34 km near the grounding line with average edge lengths of 5.7 km in the remainder of the mesh. The impact of the mesh structure and size has been tested on synthetic systems (Dow et al., 2016) and in sensitivity tests for the ASB system. While refining the mesh (as we have done) compared to an equal element mesh does cause a mean increase of $3\text{x}10^{-3}$ m in the water depth (and a maximum of 0.06 m in restricted topographic hollows, an impact of $<2\%$), the patterns of water pressure, and general locations of channels remain the same across different meshes. The time stepping within GlaDS is adaptive but we output values every 50 days. For each simulation, the model is first run to steady state, which is reached when the temporal change in water depth at every node is zero.

The GlaDS basal hydrology model calculates the distribution of subglacial water and the associated hydraulic pressures. It requires boundary conditions of the bedrock topography, ice overburden pressure, basal ice velocity to calculate cavity opening rates, and water fluxes from the base of the ice sheet. The basal and surface topography DEMs used as inputs into GlaDS are created by applying a natural interpolation to the topographic lines derived

from the ICECAP radar and surface altimetry data, respectively (Fig. 1a). Other key inputs include the basal water production rate and the basal ice flow speed. The former drives the development of the subglacial hydrological network and the latter determines the size of basal cavities that the distributed sheet flows through. It follows that the faster the ice flow speed, the larger the cavities will be and more water will be required to pressurize those cavities. To obtain basal water production rate and basal flow speed for ASB, we ran a thermomechanical ice sheet model using the Ice Sheet System Model (Larour et al., 2012, ISSM) with the same horizontal mesh as GlaDS. The ISSM model setup included surface elevation and ice sheet/shelf thickness data, which were derived from the same DEMs used as inputs into GlaDS, following which the model was initialized with MEaSURES v2 velocity data (Rignot et al., 2017). For the thermal model, surface temperature and mass balance data were derived from RACMO 2.3 output (Van Wessem et al., 2014), and the geothermal heat flux was set at a constant $55\,\mathrm{mW\,m^{-2}}$. This value compares with the Wright et al. (2012) value of $54\,\mathrm{mW\,m^{-2}}$ based on the work of Siegert and Dowdeswell (1996), and is the mean of the area-averaged geothermal heat flux estimates of $50\,\mathrm{mW\,m^{-2}}$ from Shapiro and Ritzwoller (2004) and $58\,\mathrm{mW\,m^{-2}}$ from Maule et al. (2005). We used the higher-order (Blatter, 1995; Pattyn, 2003) approximation to the full-Stokes equations for the mechanical model. The basal friction was calculated using inverse methods (e.g. MacAyeal, 1992; Morlighem et al., 2010), where the cost function included absolute and logarithmic misfits between observed and simulated velocities, as well as a regularization term that penalizes large gradients in the friction coefficient. Finally, a steady state solution, wherein

the mechanical and thermal models were allowed to evolve, provided the boundary conditions for GlaDS. The basal water production rates calculated using ISSM are a function of combined geothermal and frictional heating and ranged from 0 in the upper catchment to 0.34 $\mathrm{m\,a^{-1}}$ near the Totten Glacier grounding line (Fig. 1b). Basal sliding velocity simulated from ISSM was used as a temporally static, but spatially variable, input into GlaDS to simulate cavity opening rates. Basal sliding rates ranged from 0.06 $\mathrm{m\,a^{-1}}$ at the upper end of the catchment to 750$\mathrm{m\,a^{-1}}$ at the Totten Glacier grounding line (Fig. 1c). However, we capped the basal slip value to 500 $\mathrm{m\,a^{-1}}$ as GlaDS becomes unstable with higher velocities. Sensitivity tests on the impact of similar velocity clipping of GlaDS were applied to a semi-synthetic system representing Greenland tidewater glaciers (Poinar et al., 2019) and it was found that it had minimal impact on the catchment-wide hydrological development patterns.

Parameter values for our sensitivity tests are listed in Table 1. To test the impact of our spatially-variable basal water input parameter, we also run GlaDS with a spatially-constant melt rate input of 2 $\mathrm{mm\,a^{-1}}$, which is similar to the areally averaged water production rate from ISSM. The use of a spatially constant melt rate has previously been applied in GlaDS due to the lack of information about spatial variability of basal melt rates in many regions (e.g. Dow et al., 2018b,a; Poinar et al., 2019). Similarly, we test the impact of variable basal speed by running the model with a spatially constant basal sliding speed of 50 $\mathrm{m\,a^{-1}}$, which represents an isoline where the basal water production rates begin to increase close to the grounding line (see Fig.1b and c). The purpose of these tests is to determine the level of

control that the basal melting and basal sliding speed have on the calculated basal hydrology network. The model is also run with multiple conductivities representing different basal material consistency. Although sediment is not explicitly modeled, lower conductivity values represent scenarios where water flow is hindered, as would be expected with the presence of sediment. The three conductivity values are $1\times10^{-3}\,\mathrm{m}^{7/4}\,\mathrm{kg}^{-1/2}$, $1\times10^{-4}\,\mathrm{m}^{7/4}\,\mathrm{kg}^{-1/2}$, and $5\times10^{-5}\,\mathrm{m}^{7/4}\,\mathrm{kg}^{-1/2}$. Below this lower value, the model simulations fail to complete because the system becomes too pressurised.

Our results presented here are from model outputs after 10,000 days (approximately 27 years), which have been run until they reach steady state. One model run (spatially constant water input) did not reach steady state as it had several regions where water continues to slowly accumulate, likely due to topographic restrictions, which may be real or a result of the DEM interpolation scheme. We limit the model run period to 10,000 days due to computational expense.

3.1. Specularity content

Here we use independent data sources from radar measurements to establish the most appropriate combination of inputs for GlaDS and apply this for our analysis of the influence of hydrology on ASB system dynamics. Specularity content measurements from ice penetrating radar have been used to establish where water is present in Antarctic subglacial systems (Schroeder et al., 2013, 2015; Young et al., 2016, 2017). Using multiple radar focusing apertures, we can infer the proportions of diffuse (from rough interfaces) and specular (from smooth interfaces) energy in the along track direction, providing insight into both the flatness and anisotropy of the subglacial interface.

Distributed water systems or subglacial lakes can provide a far smoother surface than rock, sediment or channelized water systems. The advantage of the specularity content method is that it is unaffected by the englacial radar attenuation rate, which is sometimes difficult to establish as it is related to ice temperature and composition. Schroeder et al. (2013), using specularity content analysis at Thwaites Glacier, found that anisotropic water systems aligned with ice flow could be detected in the ice sheet interior, as an elevated specularity content signature in ice-flow aligned transects. Closer to the margin, despite predictions of higher basal melting and water flux, specularity content was reduced, a result consistent with channelized water flow in this environment. While Schroeder et al. (2013) was able to identify instances of subglacial channels and distributed water systems in high resolution radargrams, that study did not incorporate a formal model of subglacial hydrology that considered effective pressure. In this study, we calculated radar specularity content over ASB from the ICECAP survey lines, following the equations described in Schroeder et al. (2015), to determine where distributed water is most likely to be located and compare this to our GlaDS simulated water distribution. The errors and uncertainties associated with specularity content data are discussed in Schroeder et al. (2015) and Young et al. (2016).

4. Results

4.1. Model validation

In order to establish the most realistic model run from our suite of tests we first compare the water pressure and water depth outputs from all the

model runs with the specularity content data for validation. To achieve this comparison, we interpolate the modeled values to the same locations where radar data were collected. Specularity content is given as a relative value between 0 and 1 with values above 0.4 assumed to show regions of water and values closer to 1 having a higher likelihood of the presence of water. We perform a cost function analysis with normalised modeled water pressure data to establish the model configuration with the least error between predicted water from the model and high specularity content. The specularity content values for ASB are plotted in Figure 2 along with the interpolations along the radar lines for the basal water pressure and depth outputs for all of the model runs. For visualization purposes, only water pressure at 99% of overburden and above is plotted, assuming that conditions would need to be close to overburden, and therefore essentially flooding any rough basal topography, to be represented in specularity content outputs. Lower pressures instead suggest water is separated into cavities and would therefore produce lower specularity content data representing rougher regions. Similarly, water depths are plotted for values of 0.07 m and above as the individual cavity heights are set at 0.08 m in the model (parameter h_r), and therefore values approaching this level imply flooding of the cavities, again more likely to be represented in the specularity content data.

The highest specularity content values are found in the central trough region of ASB (see Fig.1a for basal topography). Comparing these to the water pressure results for all runs (Fig.2) and using the cost function analysis, the standard conductivity and constant water input runs have the best match. These runs have pressure close to or above overburden in the trough

region. The standard conductivity run also has some isolated regions of high pressure that line up well with isolated regions of high specularity content (for example, the upper regions of the domain). However, the constant water input run has areas of high pressure that are not seen in the specularity content data. The other runs either have no pressure close to overburden (high conductivity and spatially constant velocity) or have high pressures in different regions than suggested by the specularity content data (low conductivity). Those runs that have a close match with the water pressure, also exhibit good overlap with water depth. However, deeper water near the Totten grounding line, produced in all of the model runs, is not exhibited in the specularity content data. The main exception to the water pressure/depth correspondence is the spatially constant velocity simulations where water depth overlaps with some of the high specularity content regions despite having almost no regions with high water pressure. From these comparisons, the most appropriate model appears to be the standard conductivity run. This will now be referred to as the base model run and the sensitivity runs will be compared directly to this run.

4.2. Base model run

The steady state results for basal water pressure and water depth for the base model run are shown in Figure 3a and b. The highest water pressure is concentrated in the central troughs and towards the Totten grounding line in the region sof maximum ice velocity. The pressures reach maximums of 101% of overburden in small areas concentrated within the troughs. The deepest water can be found in similar regions, with maximum values in the central domain and around the grounding line. The depths, however, are relatively

shallow across the domain with average depths of 0.04 m; maximum water depth is 3.4 m in an area with a topographic hollow. Within the high pressure areas of the trough, the water depth is ∼0.1 m and most of the grounding line region of Totten has water depths of ∼0.07-0.1 m.

The water routing within the catchment determines how much water volume flows over the Totten grounding line rather than over the Vanderford grounding line. The discharge volume (from both the distributed sheet and the channels) into the Totten Ice Shelf cavity is $42\,m^3\,s^{-1}$ compared to $3\,m^3\,s^{-1}$ for Vanderford. The water discharge from Totten Glacier is equivalent to mass loss of $\sim 1.3\,Gt\,a^{-1}$, which is 1.8% of the 71 $Gt\,a^{-1}$ of ice mass flux from this glacier over the period 2003-2008 (Rignot et al., 2013). While the model is spinning up to steady-state, at no point does the majority of water flow transition to Vanderford; instead flux towards the Totten grounding line always dominates. Similarly, the only channels that form in the domain feed into the Totten grounding line as opposed to Vanderford. Multiple channels with discharge ranging between $2.5\,m^3\,s^{-1}$–$10\,m^3\,s^{-1}$ converge at the head of Totten Ice Shelf producing a combined discharge of $24.7\,m^3\,s^{-1}$ (Fig. 3c). These channels measure between ∼50 km and ∼150 km long and by the time they flow into the shelf cavity reach a diameter of 94 m. A smaller channel with a discharge of $\sim 1.4\,m^3\,s^{-1}$ flows into an embayment in the southeastern side of the Totten Ice Shelf cavity. This channel runs for 35 km and achieves a diameter of 2.4 m as it flows over the grounding line. The remainder of the discharge ($\sim 16\,m^3\,s^{-1}$) is fed into the ice shelf cavity through small channels and the distributed sheet.

The relationship between specularity content and the base model water

pressure and depth are plotted in Figure 5, which demonstrates that higher specularity content is more closely associated with higher water pressure than regions of deeper water. Taking 0.4 as the division where specularity content shows the presence of water (Young et al., 2016), only 1% of specularity content above this level occurs where pressures are <85% of overburden, and 15% where pressures are <95% of overburden. The median value for water pressure with high specularity content (>0.4) is 98% of overburden. In contrast, the median value for water depth associated with high specularity content is 0.067 m with 30% of high specularity content values occurring below 0.04 m depth (half the cavity depth of 0.08 m).

4.3. Model sensitivity

We compare the water pressure and depth results from all of the model runs with the base model run to determine the impact that the input variables have on the model results. With a higher conductivity (Fig. 4a,b), the water pressure is lower as the water can flow more easily through the domain. This is most prominent towards the grounding line. Similarly, water depths are ∼0.05 m shallower near the grounding line and also in the trough regions. With a lower conductivity compared to the base model run (Fig. 4c,d), water pressures are lower within the deeper trough areas and higher on the approach to the grounding line region. It is interesting to note that there is a trough region that displays high water pressure in the high conductivity run and lower pressure in the low conductivity run, which is the opposite pattern seen in the rest of the domain. This suggests that, while topography is a primary control in drainage of the upper troughs, the lower troughs are

controlled by the conductivity, which is an unknown parameter and would require independent geophysical surveys (such as active seismics) to better constrain. Compared to other runs, there is minimal impact on the steady state pressure and water depth with lower conductivity (water depth only differs by $\sim \pm 0.02\,\mathrm{m}$). In particular, the region close to the Totten Glacier grounding line has no difference in water pressure or water depth compared to the base model run. The likely reason for this is that the lower conductivity is applied to the distributed system and, in this region, channels dominate as shown in Figure 3c. Decreasing the conductivity here would cause temporary pressure increases in the distributed system and drive the water directly into the adjacent, lower pressure, channels causing the distributed water pressure to decrease again to the steady state.

With a spatially constant water input rate of $2\,\mathrm{mm\,a^{-1}}$, there are differences compared to the base model run across most of the domain (Fig. 4e,f). Water pressure is higher in many areas of the domain, primarily focused in areas outside the central troughs. Around the grounding line, however, water pressures are lower than the base model run. The water depth for the spatially constant water input has the greatest difference from the base run compared to the other sensitivity tests. Outside of the troughs, water is deeper, and near the grounding line is shallower, echoing the patterns of high and low water pressure. There are also regions where water accumulates in basal topographic dips within the troughs in the spatially constant water input run. The water depth difference plots are capped at 0.2 m for comparability but the depth difference for Figure 4 f reaches a maximum of 1.3 m, although in a very restricted region. The primary reason for this is that

water input rates across much of the domain using the ISSM values (Fig. 1c) are very low, often close to zero. A $2\,\mathrm{mm\,a^{-1}}$ input in the upper domain is an order of magnitude more water than is present in the base model run in the same regions. It should also be noted that the spatially constant water input does not reach steady state (and does not do so within the computing constraints, even if run for longer). As such, the regions of water accumulation in the trough may not be permanent steady state features but instead are likely temporary regions of filling and draining.

In comparison, the model run with basal sliding velocity everywhere at $50\,\mathrm{m\,a^{-1}}$ has a significant difference in water pressure, but limited difference in water depth (Fig. 4g,h). Water pressures are much lower compared to the base model run in most areas of the domain apart from near the grounding line. The reason for this is that faster sliding speeds open the cavities and lower the water pressure. The uniform basal sliding is too fast for the upper reaches and too slow for the grounding line, changing the basal pressure conditions. The spatial variation between higher and lower water depth in the spatially constant velocity run is greater compared to water pressure, which is uniformally lower in the up-glacier regions. This is due to the topographic influence of the troughs for draining water; in the base run, water in the troughs is much deeper than the upland regions and, with cavities opening more quickly, higher volumes of water can be pumped through the faster flux regions, increasing the efficiency and therefore lowering both pressure and water depth. In the upland regions, even with opening cavities, the connections with downstream drainage are not well established and so the faster velocity allows water buildup relative to the small water depth ($<0.05\,\mathrm{m}$) in

the base run. These relationships between topographical control and ease of water flux through the system are also demonstrated by comparing the patterns of water depth difference for the higher conductivity and uniform basal velocity model runs (Fig. 4b and h). Although they have different ranges, both difference plots show similar patterns with a decrease in water depth in the troughs and no change or increase in water depth in the highlands. There is therefore a degree of topographical control on water flux but also a strong control from the model parameters that determine water flux rates through the distributed system. These relationships illustrate the benefits of utilizing geophysical datasets to constrain the most appropriate model parameters.

5. Discussion

Subglacial hydrology models have been run in many configurations and locations (see Flowers, 2015, for an overview). A significant limitation in subglacial hydrology modeling has been the lack of data available to validate these models. Current hydrological models with coupled distributed and efficient components have made advances by initiatializing with only distributed drainage and allowing natural development of channels as the drainage system evolves (e.g. Werder et al., 2013; Hewitt, 2013; Sommers et al., 2018). The results are encouraging but continue to be limited by unknown parameters including the basal distributed system conductivity, the water input rate and the basal sliding rate. Here we address these issues by using ISSM derived basal sliding and water input rates that are spatially, although not temporally, variable, and test several values of basal conductivity. With the lack of information about patterns of conductivity we apply this parameter as

a spatially constant parameter although its variability may have implications for the basal hydrological development (Downs et al., 2018). Our analysis of the applicability of these various runs is made possible due to the specularity content data, which is a proxy for regions of distributed water at the ice-bed interface.

The results from the specularity content calculations most closely align with the water pressure records from the standard conductivity model run rather than water depth (see Fig.5). This suggests that the uplift of ice as a result of high water pressure is important for producing strong reflections identified by the radar (Schroeder et al., 2015). Regions of water that are deeper but not highly pressurised will likely be contained in cavities with the weight of the ice supported on the ridges between cavities. Those cavity ridges may cause higher refraction of radar waves and therefore lower specularity content in comparison with areas where water may be shallower but sufficiently pressurised to uplift the ice above it and drown cavities. The correspondence between the water pressure and the specularity content outputs give confidence that the model is producing a reasonable replication of the basal hydrological system, particularly in terms of the pressure, which is the most useful output for assessing ice dynamics. It is interesting that the constant water input model run overlaps well with the specularity content data, with high pressure matching high specularity content in some regions not covered by the base model run (see Fig.5a,b and h). This suggests that ISSM is producing lower rates of water production than occur in reality in the interior basin. One cause for this could be the estimated geothermal heat flux of $55\,\mathrm{mW\,m^{-2}}$, which is potentially too low for this interior region and

impacts the water production rate.

The highest basal water production and fastest ice flow velocities are found near the Totten grounding line and are closely linked features (see Fig. 1 b,c). This drives development of a network of channels that drain into the ice shelf cavity. If examining the basal hydrology from an Alpine Glacier perspective, it might be expected that the presence of large channels would slow down the ice velocity of this region, which does not appear to happen. However, in the Antarctic, where channels are fed by steady state water input rather than seasonal cycles, channels can persist close to overburden pressure and, although they prevent pressures above overburden in their vicinity, they do not substantially reduce the distributed system below overburden pressure (Dow et al., 2016, 2018b). Concentrated channel influx over the grounding line at the head of the ice shelf and, to a lesser extent, at the southeastern margin may influence ocean circulation and/or ice shelf melt rates of Totten Ice Shelf (see e.g. Xu et al., 2013).

Given the greater water depth near the Totten grounding line seen in all of the model runs (including spatially constant velocity and water input), it is perhaps surprising that the specularity content data do not also exhibit high values in a similar region; instead high specularity content is primarily restricted to the deep trough regions in the center of ASB. The region of greater water depth is consistent with a region of elevated basal reflectivity (Wright et al., 2012), although that analysis was dependent on a model of attenuation with some uncertainty. However, both of these results are consistent with the results at Thwaites Glacier (Schroeder et al., 2013; Young et al., 2016) where subglacial channels carving into the ice will act to roughen

the subglacial interface, reducing the specular component of the radar signal, while still resulting in elevated bed reflectivity due to the presence of water. As Schroeder et al. (2013) identified basal channels in similar regions using high resolution radargrams, future field campaigns in the ASB region could be directed to collecting these data.

The ability of our model simulations to inform the design of future field work is an important feedback mechanism for any well integrated modeling and observation program. Here we recommend collection of orthogonal coherent radar tracks with line spacing of less than 500 m, potentially with multiple frequencies and/or multi-polarized antennae, and focused in the regions where modeled channels form. We also suggest on-the-ground collection of high bandwidth active seismic data to determine the substrate type and porosity underneath the ice along with water depth. Following our discussion of the applicability of ISSM basal melt rates above, it would also be worthwhile using techniques such as phase-sensitive radar (ApRES) to determine basal melt rates in regions that are estimated to have low water production but produce high specularity content values. These geophysical techniques combined with the modeling would aid analysis of the role of hydrological networks near the Totten Glacier grounding line.

The modeling output comparison exercise demonstrates that the volume of water input to the bed and the basal velocity are strong controls on regions of high pressure and greater water accumulation. However, the central trough regions also have high pressure in the spatially constant water input and low conductivity runs (Fig.2). Larger water depths also seem to be concentrated within the troughs and towards the grounding line, regardless of model run.

In all model runs, the channels only form towards the Totten grounding line, with no channels flowing into Vanderford. This is explained by the partitioning of most of the ASB catchment flow towards Totten in comparison with Vanderford; this occurs for all model runs including those with spatially constant basal velocity and water production. It is likely that the flux of most of the catchment water into the Totten Glacier region is what drives the fast ice flow, resulting in higher frictional heating and therefore greater melt rates. With our spatially variable inputs, that argument would be circular except that our model runs also demonstrate the same behavior when high velocity and melt rates are not prescribed in this region (i.e. in our spatially constant water input and velocity runs). As it is, the catchment flux partition likely have an influence on the fast flow characteristics of Totten Glacier.

The future stability of Aurora Subglacial Basin is a primary motivation for examining basal hydrological conditions. Our hydrology simulations suggest that distributed systems dominate throughout the catchment except near the grounding line where large channels form. Pressures are close to (or slightly above) overburden throughout, corresponding with the areas of fastest velocity in the ASB troughs. As shown by the pressure difference maps (Fig. 4), water pressure in the troughs for the spatially constant velocity run are very close to the baseline run and therefore the input basal velocity is not the only control on high pressures in the central ASB region. Patchy areas of high and lower pressure near the Totten grounding line in all model runs demonstrates the influence of the channels on the pressure regime. These channels may play an important role in the future flow speeds of the Totten Glacier, particularly if the buttressing impact of Totten Ice

Shelf was reduced or removed. For example, steeper glacier surface slopes could encourage stronger hydraulic potential gradients resulting in larger and more efficient channel formation, perhaps causing a reduction in speed of the ice near the grounding line due to lower basal water pressures. It has previously been argued that an increase in surface slope leads to greater driving stresses and hence ice velocities (Cuffey and Paterson, 2010) and so the potential for larger, more efficient channels to offset this could have important implications for Antarctic ice dynamics. The patchy high pressure/deeper water regions may be similar to the lakes that have been identified in this region (Smith et al., 2009; Wright et al., 2012). However, with a steady state configuration, lake dynamics are not well represented and to examine these will require a focused modeling analysis of the region near the grounding line.

6. Conclusion

Aurora Subglacial Basin is an important catchment in East Antarctica and the ice in this region is currently buttressed by Totten Ice Shelf, which is becoming less stable in the presence of warming ocean waters (Greenbaum et al., 2015). We have run GlaDS subglacial hydrology model over the basin to establish steady state drainage conditions. The model is applied with spatially variable basal melt rates and basal sliding rates from ISSM. We determine the most appropriate model configuration by comparing water pressure and depth outputs with specularity content calculated from radar data that has been gathered over much of ASB. These specularity content data suggest the wettest areas of ASB are within the central troughs. This corresponds well with the water pressure estimates, although the model pro-

duces thicker water around the grounding line than would be suggested by specularity content; this is likely due to channel formation near the grounding line causing rougher specularity content. Water depth throughout the basin is shallow (generally less than 0.2 m) and pressures are close to overburden, except in the central troughs where they slightly exceed overburden. In all model runs, large basal channels form at the head of Totten Ice Shelf, draining water into the ocean cavity at rates of up to $10\,\mathrm{m}^3\,\mathrm{s}^{-1}$. These channels may influence melt rates of the ice shelf and ocean circulation. The combination of geophysical data and modeling outputs provides an ideal experiment to test the validity of the hydrology model and establish the most likely drainage conditions under ASB. The close correspondence between the specularity content data and the baseline model water pressure in particular gives confidence about the applicability of GlaDS to Antarctic drainage systems. Using these results, we recommend specific locations and types of data collection that would allow ground-truthing of our modeled observations.

7. Acknowledgments

CD was supported by a SCAR Fellowship, the Natural Sciences and Engineering Research Council of Canada and the Canada Research Chairs Program. This research was supported under Australian Research Council's Special Research Initiative for Antarctic Gateway Partnership (Project ID SR140300001) and by Australian Antarctic Division projects 3103, 4077, 4287 and 4346, NASA grant NNX09AR52G (Operation Ice Bridge), NERC grant NE/F016646/1, NERC fellowship NE/G012733/2, the Jackson School of Geoscience, the Jet Propulsion Laboratory and the G. Unger Vetlesen

Table 1: Model parameters

Parameter	Value	Units
Bedrock bump height (h_r)	0.08	m
Cavity spacing	2	m
Channel conductivity	5×10^{-2}	$m^{3/2}\,kg^{-1/2}$
Englacial void ratio	10^{-5}	
Glen's flow constant (n)	3	
Gravitational acceleration	9.81	m s^{-2}
Ice density	910	kg m^{-3}
Ice flow constant	2.5×10^{-25}	Pa^3 s^{-1}
Latent heat of fusion	3.34×10^5	J kg^{-1}
Sheet width below channel	2	m
Water density	1000	kg m^{-3}

Foundation. This research was also supported by the Australian Government's Cooperative Research Centres Programme through the Antarctic Climate & Ecosystems Cooperative Research Centre. This is UTIG contribution No. XXXX. Model inputs, outputs and specularity content data are available in Zenodo data repository (doi:10.5281/zenodo.3525474). We thank three anonymous reviewers for their helpful comments.

References

Aitken, A., Roberts, J., Van Ommen, T., Young, D., Golledge, N., Greenbaum, J., Blankenship, D., Siegert, M., 2016. Repeated large-scale retreat

564 and advance of Totten Glacier indicated by inland bed erosion. Nature
565 533, 385–389.

566 Bindschadler, R., Choi, H., Wichlacz, A., Bingham, B., Bohlander, J., Brunt,
567 K., Corr, H., Drews, R., Fricker, H., Hall, M., et al., 2011. Getting around
568 Antarctica: new high-resolution mappings of the grounded and freely-
569 floating boundaries of the Antarctic Ice Sheet created for the International
570 Polar Year. The Cryosphere 5, 569–588.

571 Blankenship, D., Kempf, S.D., Young, D.A., Richter, T.G., Schroeder, D.M.,
572 Greenbaum, J.S., van Ommen, T., Warner, R.C., Roberts, J.L., Young,
573 N.W., Lemeur, E., Siegert, M.J., 2012. IceBridge HiCARS 2 L2 Geolocated
574 Ice Thickness, Version 1. doi:10.5067/9EBR2T0VXUDG.

575 Blankenship, D., Roberts, J.L., Greenbaum, J., Young, D., Van Ommen,
576 T., Le Meur, E., Beem, L., 2018. EAGLE/ICECAP II Radargrams.
577 doi:https://doi.org/10.26179/5bcff4afc287d.

578 Blankenship, D.D., Kempf, S.D., Young, D.A., Richter, T.G., Schroeder,
579 D.M., Greenbaum, J.S., Holt, J.W., van Ommen, T., Warner,
580 R.C., Roberts, J.L., Young, N.W., Lemeur, E., Siegert, M.J.,
581 2011. IceBridge HiCARS 1 L2 Geolocated Ice Thickness, Version 1.
582 doi:10.5067/F5FGUT9F5089.

583 Blatter, H., 1995. Velocity and stress fields in grounded glaciers: a simple
584 algorithm for including deviatoric stress gradients. Journal of Glaciology
585 41, 333–344.

586 Cuffey, K.M., Paterson, W.S.B., 2010. The Physics of Glaciers. Academic
587 Press.

588 Dow, C.F., Karlsson, N.B., Werder, M.A., 2018a. Limited impact of sub-
589 glacial supercooling freeze-on for Greenland Ice Sheet stratigraphy. Geo-
590 physical Research Letters 45, 1481–1489.

591 Dow, C.F., Werder, M.A., Babonis, G., Nowicki, S., Walker, R.T., Csathó,
592 B., Morlighem, M., 2018b. Dynamics of active subglacial lakes in Recovery
593 Ice Stream. Journal of Geophysical Research: Earth Surface 123, 837–850.

594 Dow, C.F., Werder, M.A., Walker, R.T., 2016. Modeling antarctic subglacial
595 lake filling and drainage cycles. The Cryosphere 10, 1381–1393.

596 Downs, J.Z., Johnson, J.V., Harper, J.T., Meierbachtol, T., Werder, M.A.,
597 2018. Dynamic hydraulic conductivity reconciles mismatch between mod-
598 eled and observed winter subglacial water pressure. Journal of Geophysical
599 Research: Earth Surface 123, 818–836.

600 Flowers, G.E., 2015. Modelling water flow under glaciers and ice sheets. Pro-
601 ceedings of the Royal Society A: Mathematical, Physical and Engineering
602 Sciences 471, 20140907.

603 Fretwell, P., Pritchard, H.D., Vaughan, D.G., Bamber, J., Barrand, N., Bell,
604 R., Bianchi, C., Bingham, R., Blankenship, D., Casassa, G., et al., 2013.
605 Bedmap2: improved ice bed, surface and thickness datasets for Antarctica.
606 The Cryosphere 7, 375–393.

607 Fürst, J.J., Durand, G., Gillet-Chaulet, F., Tavard, L., Rankl, M., Braun,

608 M., Gagliardini, O., 2016. The safety band of Antarctic ice shelves. Nature
609 Climate Change 6, 479–482.

610 Gagliardini, O., Werder, M.A., 2018. Influence of increasing surface melt over
611 decadal timescales on land-terminating Greenland-type outlet glaciers.
612 Journal of Glaciology 64, 700–710.

613 Greenbaum, J., Blankenship, D., Young, D., Richter, T., Roberts, J., Aitken,
614 A., Legresy, B., Schroeder, D., Warner, R., Van Ommen, T., et al., 2015.
615 Ocean access to a cavity beneath Totten Glacier in East Antarctica. Nature
616 Geoscience 8, 294–298.

617 Gwyther, D., Galton-Fenzi, B., Hunter, J., Roberts, J., 2014. Simulated melt
618 rates for the Totten and Dalton ice shelves. Ocean Science 10, 267–279.

619 Hewitt, I.J., 2013. Seasonal changes in ice sheet motion due to melt water
620 lubrication. Earth and Planetary Science Letters 371, 16–25.

621 Joughin, I., Smith, B.E., Medley, B., 2014. Marine ice sheet collapse poten-
622 tially under way for the thwaites glacier basin, west antarctica. Science
623 344, 735–738.

624 Larour, E., Seroussi, H., Morlighem, M., Rignot, E., 2012. Continental scale,
625 high order, high spatial resolution, ice sheet modeling using the Ice Sheet
626 System Model (ISSM). Journal of Geophysical Research: Earth Surface
627 117, F01022.

628 Li, X., Rignot, E., Mouginot, J., Scheuchl, B., 2016. Ice flow dynamics and
629 mass loss of Totten Glacier, East Antarctica, from 1989 to 2015. Geophys-
630 ical Research Letters 43, 6366–6373.

631 MacAyeal, D.R., 1992. The basal stress distribution of Ice Stream E, Antarc-
632 tica, inferred by control methods. Journal of Geophysical Research: Solid
633 Earth 97, 595–603.

634 Maule, C.F., Purucker, M.E., Olsen, N., Mosegaard, K., 2005. Heat flux
635 anomalies in antarctica revealed by satellite magnetic data. Science 309,
636 464–467.

637 Morlighem, M., Rignot, E., Seroussi, H., Larour, E., Ben Dhia, H., Aubry, D.,
638 2010. Spatial patterns of basal drag inferred using control methods from
639 a full-Stokes and simpler models for Pine Island Glacier, West Antarctica.
640 Geophysical Research Letters 37.

641 Paolo, F.S., Fricker, H.A., Padman, L., 2015. Volume loss from Antarctic ice
642 shelves is accelerating. Science 348, 327–331.

643 Pattyn, F., 2003. A new three-dimensional higher-order thermomechanical
644 ice sheet model: Basic sensitivity, ice stream development, and ice flow
645 across subglacial lakes. Journal of Geophysical Research: Solid Earth 108,
646 2382.

647 Peters, M.E., Blankenship, D.D., Carter, S.P., Kempf, S.D., Young, D.A.,
648 Holt, J.W., 2007. Along-track focusing of airborne radar sounding data
649 from West Antarctica for improving basal reflection analysis and layer
650 detection. IEEE Transactions on Geoscience and Remote Sensing 45, 2725–
651 2736.

652 Poinar, K., Dow, C.F., Andrews, L.C., 2019. Long-term support of an ac-

tive subglacial hydrologic system in Southeast Greenland by firn aquifers. Geophysical Research Letters 46, 4772–4781.

Pritchard, H.D., Arthern, R.J., Vaughan, D.G., Edwards, L.A., 2009. Extensive dynamic thinning on the margins of the Greenland and Antarctic ice sheets. Nature 461, 971–975.

Rignot, E., Jacobs, S., Mouginot, J., Scheuchl, B., 2013. Ice-shelf melting around Antarctica. Science 341, 266–270.

Rignot, E., Mouginot, J., Scheuchl, B., 2017. MEaSUREs InSAR-based Antarctica ice velocity map, version 2. Boulder, CO: NASA DAAC at the National Snow and Ice Data Center .

Ritz, C., Edwards, T.L., Durand, G., Payne, A.J., Peyaud, V., Hindmarsh, R.C., 2015. Potential sea-level rise from Antarctic ice-sheet instability constrained by observations. Nature 528, 115–118.

Roberts, J., Galton-Fenzi, B.K., Paolo, F.S., Donnelly, C., Gwyther, D.E., Padman, L., Young, D., Warner, R., Greenbaum, J., Fricker, H.A., et al., 2018a. Ocean forced variability of Totten Glacier mass loss. Geological Society, London, Special Publications 461, 175–186.

Roberts, J.L., Blankenship, D.D., Grennbaum, J.S., Beem, L.H., Young, D.A., Van Ommen, T., Le Meur, E., 2018b. EAGLE/ICECAP II geophysical observations (surface and bed elevation, ice thickness, gravity disturbance and magnetic anomalies). doi:10.26179/5BCFFFDABCF92.

Schroeder, D.M., Blankenship, D.D., Raney, R.K., Grima, C., 2015. Estimating subglacial water geometry using radar bed echo specularity: applica-

tion to Thwaites Glacier, West Antarctica. IEEE Geoscience and Remote Sensing Letters 12, 443–447.

Schroeder, D.M., Blankenship, D.D., Young, D.A., 2013. Evidence for a water system transition beneath Thwaites Glacier, West Antarctica. Proceedings of the National Academy of Sciences 110, 12225–12228.

Shapiro, N.M., Ritzwoller, M.H., 2004. Inferring surface heat flux distributions guided by a global seismic model: particular application to antarctica. Earth and Planetary Science Letters 223, 213–224.

Siegert, M.J., Dowdeswell, J.A., 1996. Spatial variations in heat at the base of the antarctic ice sheet from analysis of the thermal regime above subglacial lakes. Journal of Glaciology 42, 501–509.

Siegert, M.J., Kulessa, B., Bougamont, M., Christoffersen, P., Key, K., Andersen, K.R., Booth, A.D., Smith, A.M., 2018. Antarctic subglacial groundwater: a concept paper on its measurement and potential influence on ice flow. Geological Society, London, Special Publications 461, 197–213.

Silvano, A., Rintoul, S.R., Peña-Molino, B., Williams, G.D., 2017. Distribution of water masses and meltwater on the continental shelf near the totten and moscow university ice shelves. Journal of Geophysical Research: Oceans 122, 2050–2068.

Smith, B.E., Fricker, H.A., Joughin, I.R., Tulaczyk, S., 2009. An inventory of active subglacial lakes in Antarctica detected by ICESat (2003–2008). Journal of Glaciology 55, 573–595.

Sommers, A., Rajaram, H., Morlighem, M., 2018. SHAKTI: Subglacial Hydrology and Kinetic, Transient Interactions v1. 0. Geoscientific Model Development 11, 2955–2974.

Van Wessem, J., Reijmer, C., Morlighem, M., Mouginot, J., Rignot, E., Medley, B., Joughin, I., Wouters, B., Depoorter, M., Bamber, J., et al., 2014. Improved representation of east antarctic surface mass balance in a regional atmospheric climate model. Journal of Glaciology 60, 761–700.

Werder, M.A., Hewitt, I.J., Schoof, C.G., Flowers, G.E., 2013. Modeling channelized and distributed subglacial drainage in two dimensions. Journal of Geophysical Research: Earth Surface 118, 2140–2158.

Wright, A., Young, D., Roberts, J., Schroeder, D., Bamber, J., Dowdeswell, J., Young, N., Le Brocq, A., Warner, R., Payne, A., et al., 2012. Evidence of a hydrological connection between the ice divide and ice sheet margin in the Aurora Subglacial Basin, East Antarctica. Journal of Geophysical Research: Earth Surface 117.

Xu, Y., Rignot, E., Fenty, I., Menemenlis, D., Flexas, M.M., 2013. Subaqueous melting of Store Glacier, west Greenland from three-dimensional, high-resolution numerical modeling and ocean observations. Geophysical Research Letters 40, 4648–4653.

Young, D.A., Roberts, J.L., Ritz, C., Frezzotti, M., Quartini, E., Cavitte, M.G., Tozer, C.R., Steinhage, D., Urbini, S., Corr, H.F., et al., 2017. High-resolution boundary conditions of an old ice target near Dome C, Antarctica. The Cryosphere 11, 1897–1911.

721 Young, D.A., Schroeder, D., Blankenship, D., Kempf, S.D., Quartini, E.,
722 2016. The distribution of basal water between Antarctic subglacial lakes
723 from radar sounding. Philosophical Transactions of the Royal Society A:
724 Mathematical, Physical and Engineering Sciences 374, 20140297.

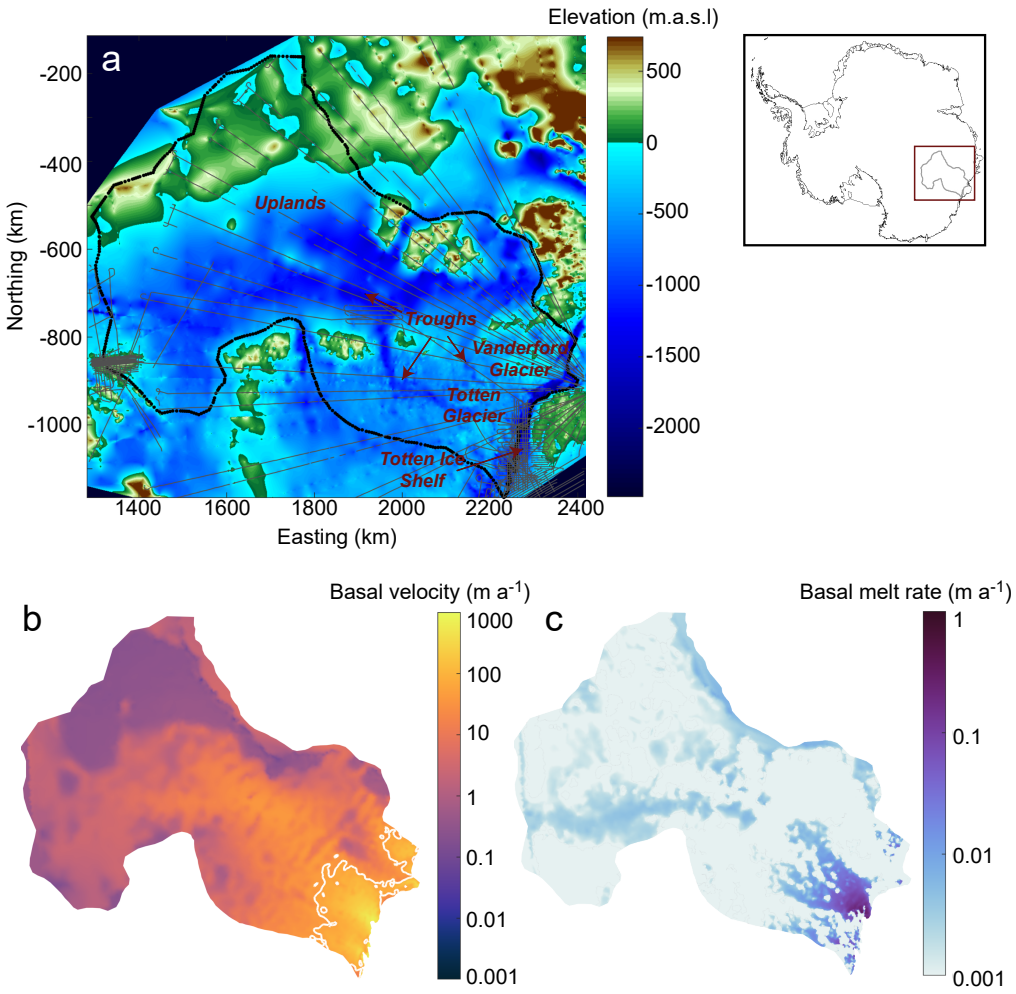


Figure 1: Aurora Subglacial Basin feeding into Totten and Vanderford Glaciers. a) Basal topography interpolated from ICECAP aerial radar data, which are plotted in gray. Elevations are relative to the WGS84 datum surface. The subset shows the location of the hydrological catchment in East Antarctica. b) Basal velocity calculated using ISSM; the white line shows the $50\,\mathrm{m\,a^{-1}}$ velocity contour. c) Basal melt rate also calculated using ISSM.

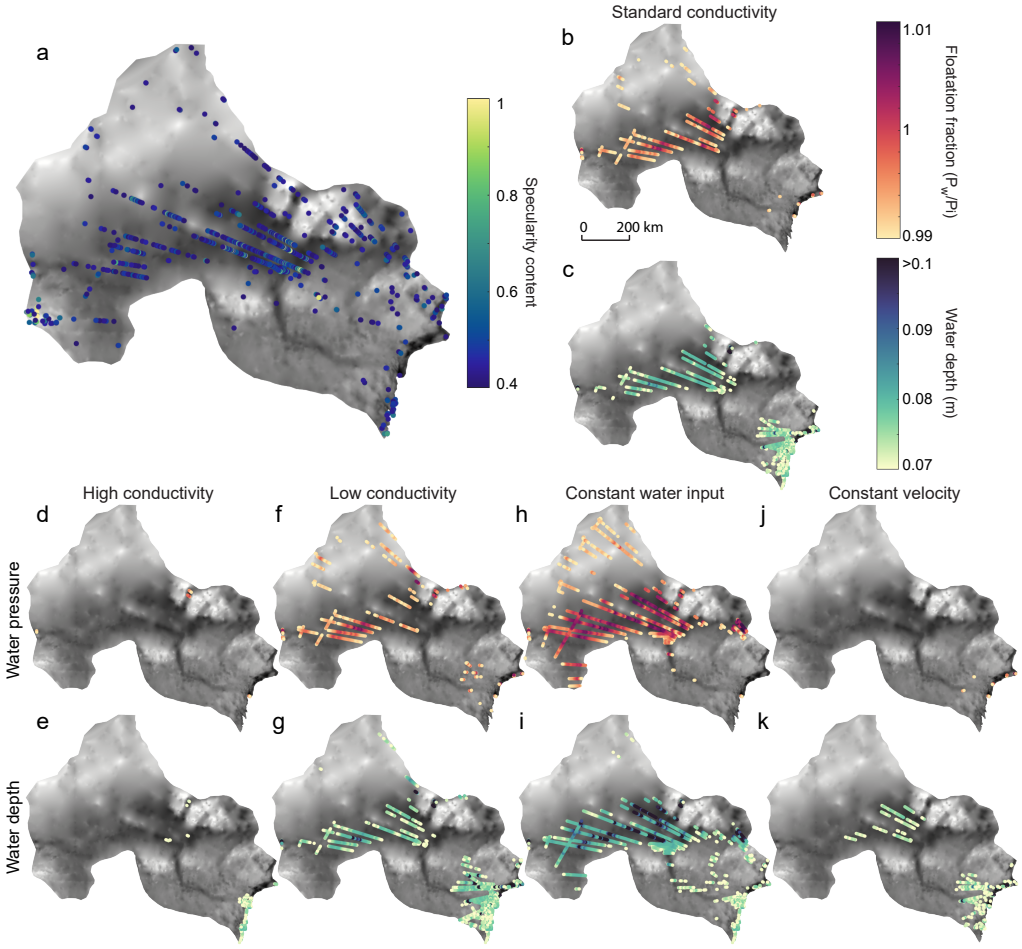


Figure 2: a) Specularity content derived from radar data collected by ICECAP plotted for levels between 0.4 and 1, representing likely presence of basal water. The background map is the basal topography b-k) water pressure and water depth plotted along the same lines as the specularity content data for comparison with a) for the base run (standard conductivity) and the various sensitivity tests.

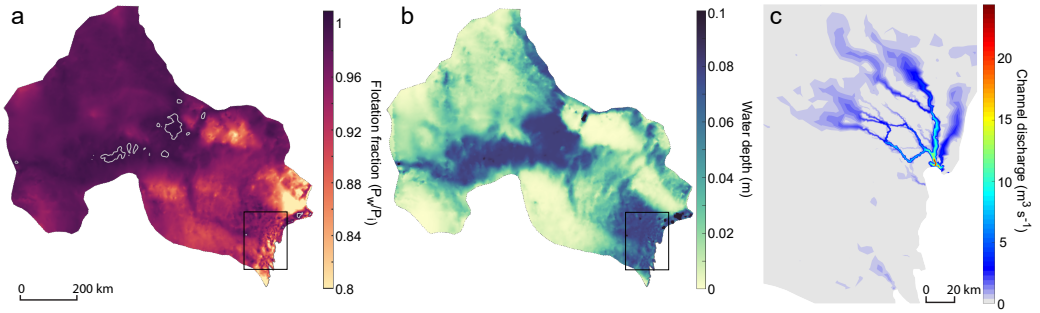


Figure 3: Base model outputs for a) water pressure, plotted as a fraction of overburden, b) water depth, capped at 0.1 m, and c) channel discharge over the Totten Glacier grounding line. The black rectangles in a) and b) show the extent of c)

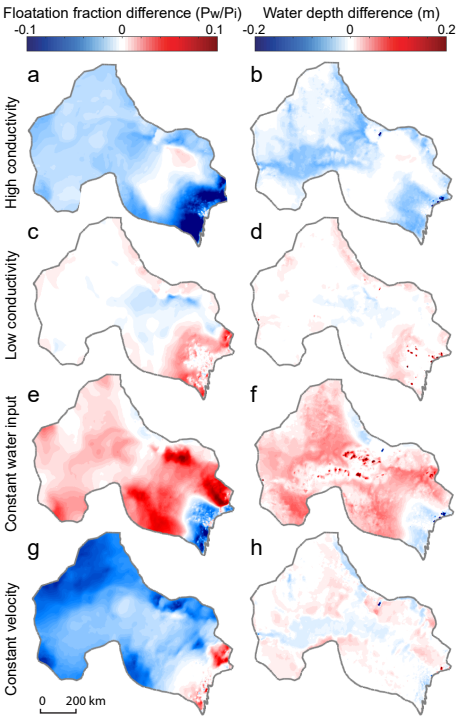


Figure 4: Difference in water pressure (as a fraction of overburden) between the base model run and a) higher conductivity, b) lower conductivity, c) spatially constant water source, and d) spatially constant basal velocity. Difference in water depth between base model run and e) higher conductivity, f) lower conductivity, g) spatially constant water source, and h) spatially constant basal velocity

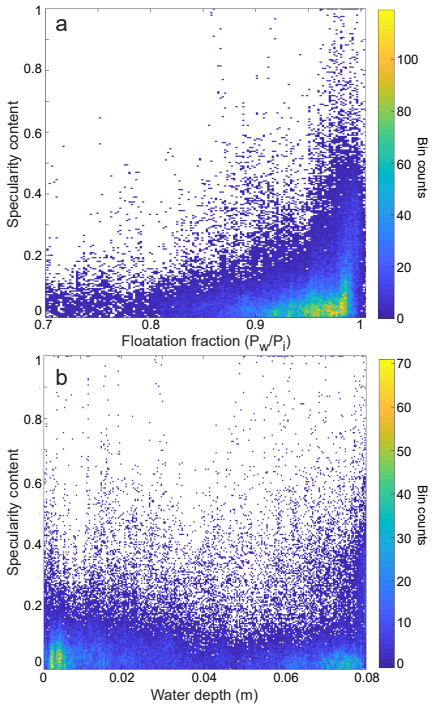


Figure 5: Color-density plots of a) water pressure and specularity content and b) water depth and specularity content. Bin counts and corresponding colors indicate the density of data points. The water pressure and depth outputs are from the base model run.